# Controlling Dynamics of Postcollision Interaction

Anton N. Artemyev, Alexej I. Streltsov, and Philipp V. Demekhin*
*Institut für Physik und CINSaT, Universität Kassel, Heinrich-Plett-Straße 40, 34132 Kassel, Germany*

(Received 8 January 2019; revised manuscript received 6 March 2019; published 7 May 2019)

A general scheme to get insight and to control postcollision interaction (PCI) by means of sequential double ionization with two high-frequency pulses is discussed. In particular, we propose to consider PCI of a slow photoelectron released by the pump pulse from a neutral atom with a fast photoelectron released by the time-delayed probe pulse from the created ion. This scheme is exemplified by the *ab initio* calculations performed for the prototypical helium atom. In order to visualize PCI effects in real time and real space, the corresponding time-dependent Schrödinger equation is solved by propagating two-electron wave packets in terms of essential stationary eigenstates of the unperturbed Hamiltonian. It is demonstrated that the exchange of energy between the slow and fast photoelectron wave packets in continuum, as well as the recapture of threshold photoelectrons owing to the PCI, can be controlled by the properties of the ionizing pulses and the time delay between them.

DOI: 10.1103/PhysRevLett.122.183201

Postcollision interaction (PCI) is a general effect of the exchange of energy between a slow primary electron released from a system and a fast secondary electron emitted by the decay of the created ion [1,2]. This effect can be considered as a special case of the long-range Coulomb interaction, and it provides fundamental information on the correlated dynamics of the unbound electrons in continuum. Since the early 1960s, PCI has been a subject of numerous experimental and theoretical studies (for more details on early studies of PCI, see Ref. [1] and Chap. 4.3.4 in the review Ref. [2]). A traditional scheme to study PCI is to consider the inner-shell photoionization of an atom which is followed by the Auger decay of the created core hole. Here, the interaction between a high-energy Auger electron and a slow photoelectron (i) results in equivalent energy shifts of the maxima of the photoelectron and Auger electron lines in two opposite directions, (ii) changes the shape of both electron spectra, and (iii) induces the recapture of the threshold photoelectrons by the ion into bound states. Because of its importance for our understanding of the electronic structure of matter, this effect is the subject of many studies up to now (see, e.g., recent works on PCI in the Auger decay of atoms [3–5], molecules [6], dimers [7,8], and clusters [9], as well as on PCI in the two-electron decay [10] and on the field-assisted PCI [11,12]).

Classically, a PCI in inner-shell photoionization can be interpreted as a sudden change in the mutual screening of the outgoing electrons [13,14]. In particular, at the instant of the emission of the Auger electron, it sees a doubly charged ion, while the photoelectron experiences an attraction of a singly charged ion. After the fast Auger electron outstripped the slow photoelectron, this picture changes, and the photoelectron shields now a doubly charged ion for the Auger electron. As a consequence, the Auger electron gains energy and the photoelectron loses the same amount of energy. The energy gain or loss depends on the distance to the nuclei $r_0$ where two electrons met, and it can be estimated in atomic units as $\Delta E \simeq 2/r_0 - 1/r_0 = 1/r_0$. In addition to this simplified classical picture, there are semiclassical approaches [15,16], the stationary quantum theory of final-state interaction of continuum electrons [17], the time-dependent perturbation theory [18], and a two-step dynamical launch model [19]. However, none of the available models of PCI [20] provide an exact and full quantum dynamical picture of the effect. Finally, the lifetime of the decay and the kinetic energy of the fast Auger electron are inherent properties of the system, which are hard to manipulate. Therefore, the kinetic energy of a slow photoelectron is the only free parameter to control PCI in the traditional scheme.

Here, we propose a more flexible and general scheme to investigate and to control PCI effects by two high-frequency, pump and probe, pulses. The process under investigation is schematically illustrated in Fig. 1 on the example of a helium atom. For simplicity, we consider the sine-squared pulses with the time envelope $g_i(t) = \sin^2(\pi t/T_i)$, which has a well-defined beginning, end, and full duration $T_i$. The pump pulse with the carrier frequency $\omega_1$ ionizes the neutral He atom from its ground state and produces slow photoelectrons with the kinetic energy of $\varepsilon_1 = \omega_1 - \mathrm{IP}$ (where IP stands for the ionization potential). After the time delay $\tau$, the probe pulse with the carrier frequency $\omega_2$ ionizes the $He^+$ ion and produces fast photoelectrons with the kinetic energy of $\varepsilon_2 = \omega_2 - \mathrm{DIP}$ (where DIP stands for the double-ionization potential). In this scheme, PCI effects in the coincidence spectrum of two

 

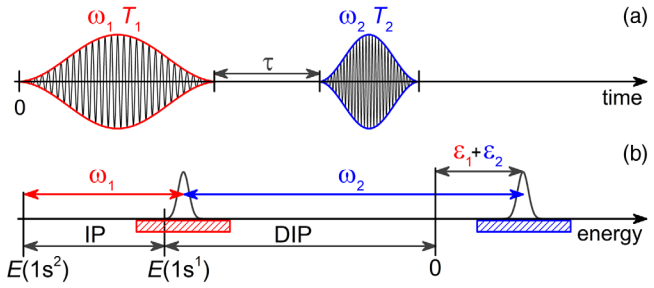


FIG. 1. (a) Scheme of the double ionization of He by the sequence of two delayed high-frequency pulses. (b) Energy scheme of the process. The pump pulse of the duration $T_1$ and carrier frequency $\omega_1$ promotes one of the two electrons of He into the near-threshold continuum, generating thereby slow photoelectrons with the kinetic energy of around $\varepsilon_1 = \omega_1 - \mathrm{IP}$. After a time delay $\tau$, the probe pulse of the duration $T_2$ and sufficient carrier frequency $\omega_2$ ionizes the $He^+$ ion and generates fast photoelectrons of the energy of $\varepsilon_2 = \omega_2 - \mathrm{DIP}$. The neutral ground state $\mathrm{He}(1s^2)$, the singly excited or ionized states centered around the energy $E(1s^2) + \omega_1$, and the doubly excited or ionized states centered around the energy $E(1s^2) + \omega_1 + \omega_2$ (both marked by the horizontal hatched rectangles) are essential for the considered process.

photoelectrons can be controlled by means of many degrees of freedom, i.e., by the parameters $T_1, \omega_1, T_2, \omega_2, \tau$, and the pulses' polarization. Importantly, high-frequency pulses required for such experiments can be produced by the high-order harmonic generation (HHG) techniques [21,22]. At present, HHG techniques allow one to generate pulses with carrier frequencies up to 110 eV (which is sufficient to ionize ions), to access peak intensities of up to $5 \times 10^{14}$ W/cm$^2$, and to suppress pulse durations down to subfemtoseconds.

In order to exemplify our idea, we performed full quantum dynamical calculations for the prototypical two-electron atom and visualized expected PCI effects in real time and real space. For this purpose, we solved the time-dependent Schrödinger equation for a He atom exposed to the linearly polarized pump and probe pulses (both polarized along the $z$ axis). In the dipole velocity gauge, the total Hamiltonian of the system reads (in atomic units)

$$\hat{H}(\vec{r},\vec{r}',t) = -\frac{1}{2}\vec{\nabla}^2 - \frac{1}{2}\vec{\nabla}'^2 - \frac{2}{r} - \frac{2}{r'} + \frac{1}{|\vec{r}-\vec{r}'|} - i(\nabla_z + \nabla_{z'})[\mathcal{A}_1 g_1(t)\sin(\omega_1 t) + \mathcal{A}_2 g_2(t)\sin(\omega_2 t)]. \quad (1)$$

Here, $\mathcal{A}_i$ are the vector potential amplitudes (the vector potential is related to the electric field via $\mathbf{E} = -\partial_t \mathbf{A}$).

An exact solution of the problem at hand including all processes evoked by two pulses is a formidable task, even for a He atom. Therefore, in order to describe PCI effects as accurately as possible, we restricted our consideration to the essential processes only. In particular, we allowed for the one-photon ionization of the neutral He by the pump pulse and for the subsequent one-photon ionization of the created $He^+$ ion by the probe pulse. We, therefore, neglected the other possible processes, such as (i) the absorption of several photons from one of the pulses and (ii) the ionization of the neutral He atoms (which survive after the pump pulse) by the probe pulse. In order to justify approximation (i), we reduced intensities of the pump and probe pulses and ensured linear regimes in each of the ionization steps. In particular, only a small fraction of around 1% of the neutral He atoms was ionized by the pump pulse, and only a small fraction of around 1% of the created $He^+$ ions was further ionized by the probe pulse. Thus, the essential two-photon absorption process forms a coincident spectrum which yields about 0.01% of all events. Thereby, the weak multiphoton processes (i) do not interfere with the essential process. Finally, the rather probable one-photon–one-electron ionization process (ii) does not interfere with essential events at all.

In the present work, we solved the time-dependent Schrödinger equation with the total Hamiltonian (1) in terms of the stationary eigenstates of the unperturbed Hamiltonian of helium by implying the following ansatz for the total wave function:

$$\Psi(\vec{r},\vec{r}',t) = a_{\epsilon_0}(t)\Phi_{\epsilon_0}(\vec{r},\vec{r}') + \sum_{\epsilon'} b_{\epsilon'}(t)\Phi_{\epsilon'}(\vec{r},\vec{r}') + \sum_{\epsilon} c_{\epsilon}(t)\Phi_{\epsilon}(\vec{r},\vec{r}'). \quad (2)$$

As justified above, this ansatz includes only selected relevant eigenstates which are essential to follow the dynamics of PCI in the considered process. In particular, it includes the wave function $\Phi_{\epsilon_0}$ of the neutral ground state with the energy $\epsilon_0 = E(1s^2)$, the singly excited or ionized states $\Phi_{\epsilon'}$ from the energy interval of $\epsilon' = E(1s^2) + \omega_1 \pm 5$ eV, and the doubly excited or ionized states $\Phi_{\epsilon}$ from the energy interval of $\epsilon = E(1s^2) + \omega_1 + \omega_2 \pm 5$ eV [indicated in Fig. 1(b) by hatched rectangles].

The spatial parts of the stationary wave functions of He with well-defined total orbital angular momentum $L$, its projection $M = 0$, and total spin $S = 0$ were sought in the two-particle basis of symmetrized pair-products of all one-particle basis functions [note that Hamiltonian (1) preserves the total spin $S$ and projection $M$ of the $^1S$ ground state of He]. The one-particle basis was built in a box via the three-dimensional finite-element discrete-variable representation [23–26] employing the normalized Lagrange polynomials constructed over a Gauss-Lobatto radial grid [27–29]. This choice has the following advantages. First, all matrix elements of the Hamiltonian (1) have closed analytic expressions, which can be found in our previous works [24,25]. Second, the Hamiltonian matrix splits in blocks according to the total angular momentum $L$. Third and important, the chosen basis results in a banded structure of the total Hamiltonian, such that about 99.9% of all matrix elements are zeros.

The matrix of the unperturbed Hamiltonian of He, constructed in the described-above two-particle basis, was diagonalized by the FEAST solver package [30,31], which provides accurate eigenstates of sparse matrices within a given interval of eigenvalues. In the calculations, we used the box size of 500 a.u., which was divided into 200 finite elements with the length of 2.5 a.u., each covered by ten Gauss-Lobatto points. The one-particle basis included partial harmonics with $\ell, |m| \leq 3$. In the weak-field limit, the ionization of the $\Phi_{\epsilon_0}(^1S)$ ground state of He by the pump pulse populates the singly ionized states $\Phi_{\epsilon'}(^1P)$. The subsequent ionization of those states by the probe pulse produces manyfold of the doubly ionized states $\Phi_{\epsilon}(^1S/^1D)$. One can independently search for the $\Phi_{\epsilon'}(^1P)$ solutions in the required energy interval of $\epsilon' = E(1s^2) + \omega_1 \pm 5$ eV and separately for the $\Phi_{\epsilon}(^1S)$ and for the $\Phi_{\epsilon}(^1D)$ solutions in the interval of $\epsilon = E(1s^2) + \omega_1 + \omega_2 \pm 5$ eV.

The present calculations yield the following energies of the ground neutral and ionic states of He: $E(1s^2) = -2.9033$ a.u. and $E(1s^1) = -2.0000$ a.u. Thereby, the theoretical IP = 24.58 eV and DIP = 54.42 eV are in very good agreement with the experimental values of 24.59 and 54.42 eV [32], respectively. In all dynamical calculations, the carrier frequencies of the pump and probe pulses were set to $\omega_1 = 26.09$ eV and $\omega_2 = 64.47$ eV, respectively [33]. Thereby, the maximum in the reference spectrum of slow photoelectrons, computed for the ionization of neutral He by the pump pulse only, was set to $\varepsilon_1 = 1.5$ eV, and the maximum in the reference spectrum of fast photoelectrons, computed for the ionization of the $He^+$ ion by the probe pulse only, to $\varepsilon_2 = 10$ eV. The full duration of the probe pulse was fixed to $T_2 = 2$ fs. In order to demonstrate a possibility to control emerging PCI effects, we used different pump pulses and time delays between the pulses.

We first discuss the temporal evolution of the one-electron radial density. As explained above, PCI effects can be found in the coincident photoelectron wave packet, which is described by the last term in the ansatz (2). The required temporal evolution can thus be obtained via

$$P(r,t) = r^2 \int d\Omega_r \int d^3\vec{r}' \left| \sum_{\epsilon} c_{\epsilon}(t) \Phi_{\epsilon}(\vec{r},\vec{r}') \right|^2. \quad (3)$$

The results of the present calculations, performed for the pump pulse of full duration $T_1 = 5$ fs and two different time delays of $\tau = 1$ and 3 fs, are summarized in Fig. 2. We note that the coincident part of the ansatz (2) can be populated only after the probe pulse has began at $t = T_1 + \tau$, and its population is completed after the probe pulse has ended at $t = T_1 + \tau + T_2$. Therefore, Fig. 2 follows free evolutions of the created two-electron wave packets starting from the end of the probe pulse.

As one can see from Fig. 2, the early two-electron wave packets (at 8 fs in the upper and at 10 fs in the lower panels) consist of two humps. The slow photoelectrons, generated at earlier times, are located at larger distances, and the fast photoelectrons, generated at later times, at smaller. As the time evolves, the wave packet of fast photoelectrons runs after, passes through, and then overtakes the wave packet of slow photoelectrons. At later times (16 fs in the upper and 20 fs in the lower panels), the fast photoelectrons are located at larger and the slow one at smaller distances. The two wave packets meet at different places, which can be controlled by the time delay $\tau$. Indeed, they meet at $r = 130$ a.u. and $t = 10.5$ fs for $\tau = 1$ fs (upper panel in Fig. 2) and at $r = 180$ a.u. and $t = 13.75$ fs for $\tau = 3$ fs (lower panel in Fig. 2). More details on the time evolution of radial density can be found in Supplemental Material [34].

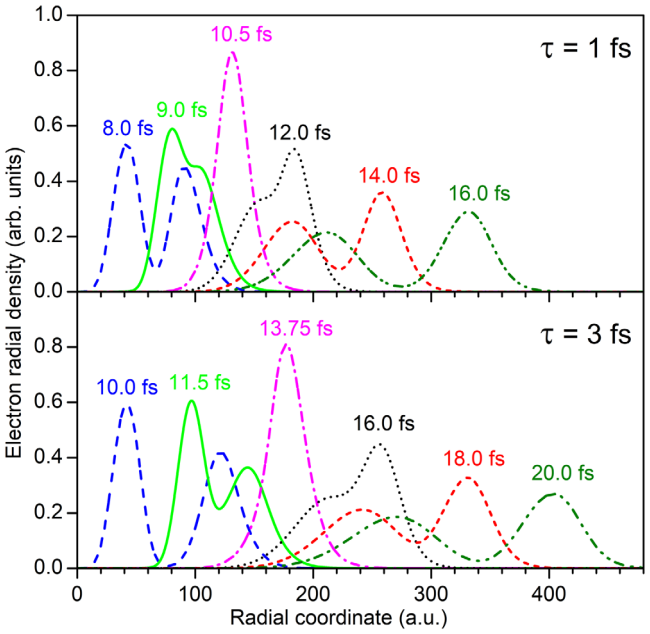


FIG. 2. One-electron radial density (3) computed for the double ionization of He by the sequence of two high-frequency pulses at different times (indicated near each curve). The pump pulse with duration $T_1 = 5$ fs and carrier frequency $\omega_1 = 26.09$ eV generates slow photoelectrons with the kinetic energy of around $\varepsilon_1 = 1.5$ eV, while the probe pulse with $T_2 = 2$ fs and $\omega_2 = 64.47$ eV creates fast photoelectrons with $\varepsilon_2 = 10$ eV. Right after the second pulse has ended, the wave packet of slow photoelectrons is located at somewhat larger distances, while that of the fast photoelectrons at smaller distances. As the time proceeds, the fast photoelectrons overtake the slow ones. Depending on the time delay between two pulses, the two wave packets meet at different distances: at about 130 a.u. for $\tau = 1$ fs in the upper panel and at about 180 a.u. for $\tau = 3$ fs in the lower panel. As a consequence, two electrons exchange by different portions of energy via PCI.

We now analyze the coincident energy spectrum of the photoelectrons. In order to follow the time evolution of the spectrum, we project here the coincident spatial wave packet on the Coulomb waves:

$$W(\vec{k},\vec{k}',t)=\frac{1}{(2\pi)^3}\Bigg|\int d^3\vec{r}\times\left(\int_{r'\le r}d^3\vec{r}'\psi_C^{-*}(\vec{k},\vec{r},1)\psi_C^{-*}(\vec{k}',\vec{r}',2)+\int_{r'>r}d^3\vec{r}'\psi_C^{-*}(\vec{k},\vec{r},2)\psi_C^{-*}(\vec{k}',\vec{r}',1)\right)\times\sum_\epsilon c_\epsilon(t)\Phi_\epsilon(\vec{r},\vec{r}')\Bigg|^2, \quad (4)$$

where $\psi_C^-(\vec{k},\vec{r},Z)$ are the incoming-wave momentum-normalized superpositions of the spherical Coulomb waves [35]. Equation (4) ensures that photoelectrons which are located closer to the nucleus are projected on the Coulomb waves with $Z=2$, and those located farther to the nucleus on the waves with $Z=1$. For instance, in the early coincident spectrum at the very beginning, the wave packets of slow photoelectrons are projected on Coulomb waves with $Z=1$, and those of fast photoelectrons on the waves with $Z=2$. On the contrary, the final coincident spectrum is obtained by projecting the wave packets of slow electrons on Coulomb waves with $Z=2$, and those of fast electrons on the waves with $Z=1$.

Figure 3 demonstrates electron energy spectra obtained for the final two-electron wave packets shown in Fig. 2. Those one-electron spectra were obtained from the coincident spectrum (4) via the following projection:

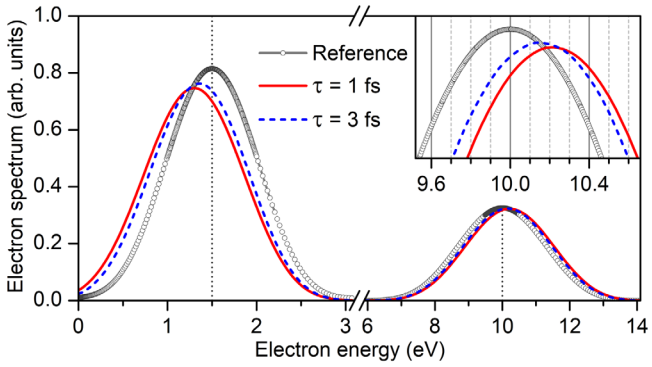


FIG. 3. Final photoelectron spectra (5) of He computed for the combinations of two pulses with $T_1=5$ fs, $\omega_1=26.09$ eV and $T_2=2$ fs, $\omega_2=64.47$ eV and two different time delays $\tau=1$ and 3 fs (see the legend). The spectrum of slow electrons computed for the ionization of He by the pump pulse only (with the maximum at $\varepsilon_1=1.5$ eV) and the spectrum of fast electrons computed for the ionization of the $He^+$ ion by the probe pulse only (with the maximum at $\varepsilon_2=10$ eV) are shown for reference. The inset illustrates the maximum of the spectrum of fast electrons on an enlarged scale. One can see that PCI results in the exchange of energy between the slow and fast electrons, such that the energy of slow electrons decreases and that of the fast increases. For time delays $\tau=1$ and 3 fs, the energy shifts of about $\pm0.21$ and $\pm0.15$ eV suggest that two wave packets meet at about 130 and 180 a.u., respectively (see also Fig. 2 and its caption).

$$\mathcal{W}(\varepsilon,t)=k\int d\Omega_k\int d^3\vec{k}'W(\vec{k},\vec{k}',t), \quad (5)$$

with the electron kinetic energy $\varepsilon=k^2/2$. The reference spectra of slow and fast photoelectrons, computed for each pulse separately, are also shown for comparison. Those reference spectra coincide with the one-electron spectra obtained from the early coincident spectrum, where wave packets of slow electrons are projected on Coulomb waves with $Z=1$, and those of fast electrons on waves with $Z=2$. One can see from Fig. 3 that the maximum of the final spectrum of slow photoelectrons systematically shifts towards lower kinetic energies, while that of the spectrum of fast photoelectrons toward higher energies, as compared to the respective reference spectra. The energy shifts are larger (smaller) if the wave packets meet at smaller (larger) distances. The present results agree with the classical estimate via the $\Delta E\simeq 1/r_0$ formula. Indeed, the energy shifts of $\pm0.21$ and $\pm0.15$ eV, observed for the time delays $\tau=1$ and 3 fs at the maxima, suggest that the wave packets meet at about 130 and 180 a.u., respectively. Since different parts of the coincident wave packet meet at different distances, PCI results in notable deformations of the shape of each spectrum. Complete time-evolutions of the photoelectron spectra from Fig. 3 can be found in the Supplemental Materials [34].

Let us, finally, have a closer look at the threshold part of the spectrum of slow photoelectrons in Fig. 3. Owing to substantial losses of energy caused by PCI, a part of the very slow photoelectrons acquired negative kinetic energies. In other words, they became recaptured to bound states of the $He^+$ ion. As one can see from Fig. 3, the effect of recapture is different for different time delays $\tau$.

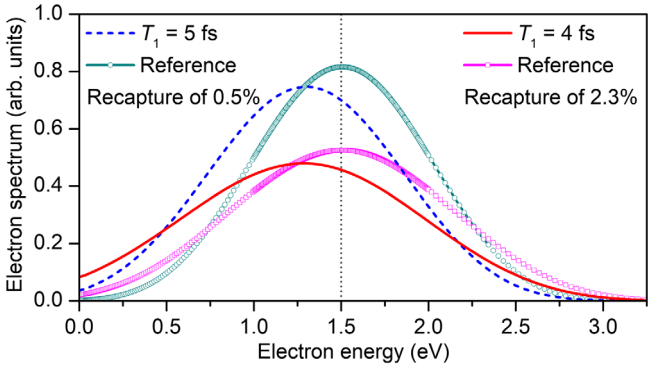


FIG. 4. Final spectra (5) of slow photoelectrons computed for the ionization of He by different combinations of two pulses with $\omega_1=26.09$ eV, $\omega_2=64.47$ eV, and time delay $\tau=1$ fs. The second pulse has duration $T_2=2$ fs, while the first one $T_1=4$ or 5 fs (see the legends). The respective spectra of slow electrons computed for the ionization of He by the first pulse only (with the maximum at $\varepsilon_1=1.5$ eV) are shown for reference. As is clearly seen from the computed spectra at $\varepsilon_1\approx0$, a part of the threshold photoelectrons (indicated in percent in each legend) is recaptured by the doubly charged ion to produce bound states of the singly charged ion, which is owing to the PCI with fast photoelectrons.

Obviously, the effects of recapture can also be controlled by other parameters. Figure 4 illustrates this fact for two different durations $T_1 = 4$ and 5 fs of the pump pulse, while the time delay $\tau = 1$ fs and duration of the probe pulse $T_2 = 2$ fs were kept fixed. One can see that a significantly larger portion of about 2.3% of the threshold photoelectrons is recaptured for the shorter pump pulse, as compared to 0.5% for the longer (compare also each final spectrum with the respective reference spectrum).

In conclusion, we propose to study PCI effects by experiments on a double ionization of atoms with two delayed high-frequency pulses and exemplify our suggestion by the full dynamical calculations for helium. In contrast to the traditional scheme involving photoelectrons and Auger electrons, the wave packets of two photoelectrons are emitted coherently which opens a playground for new interference effects, e.g., in the angular correlation [3,19,36] of the entangled photoelectrons. The theoretically demonstrated possibility to manipulate PCI by the durations, carrier frequencies, and time delay of the pump and probe pulses opens a door to the diverse control of such coherent PCI effects in experiments at present HHG facilities. Our *ab initio* theoretical approach, which relies on the quantum dynamical propagation of two-active-electron wave packets, can straightforwardly be extended to atoms with more electrons. It substantially advances the theory of PCI beyond available theoretical models and allows one to follow the temporal evolution of highly differential coincident observables. As an illustration, Supplemental Material [34] includes animations: (i) how fast photoelectrons emitted in a particular direction penetrate through the density of slow photoelectrons and (ii) how the density of fast photoelectrons scatters on slow photoelectrons emitted in a particular direction. Those animations demonstrate an intricate patterning of the photoelectron density evoked by the coherent scattering processes.

This work was supported by the Deutsche Forschungsgemeinschaft (DFG).

*demekhin@physik.uni-kassel.de


[1] V. Schmidt, AIP Conf. Proc. **94**, 544 (1982).
[2] V. Schmidt, Rep. Prog. Phys. **55**, 1483 (1992).
[3] A. L. Landers *et al.*, Phys. Rev. Lett. **102**, 223001 (2009).
[4] R. Guillemin, S. Sheinerman, C. Bomme, L. Journel, T. Marin, T. Marchenko, R. K. Kushawaha, N. Trcera, M. N. Piancastelli, and M. Simon, Phys. Rev. Lett. **109**, 013001 (2012).
[5] R. Guillemin, S. Sheinerman, R. Püttner, T. Marchenko, G. Goldsztejn, L. Journel, R. K. Kushawaha, D. Céolin, M. N. Piancastelli, and M. Simon, Phys. Rev. A **92**, 012503 (2015).
[6] D. L. Hansen, G. B. Armen, M. E. Arrasate, J. Cotter, G. R. Fisher, K. T. Leung, J. C. Levin, R. Martin, P. Neill, R. C. C. Perera, I. A. Sellin, M. Simon, Y. Uehara, B. Vanderford, S. B. Whitfield, and D. W. Lindle, Phys. Rev. A **57**, R4090 (1998).
[7] F. Trinter *et al.*, Phys. Rev. Lett. **111**, 093401 (2013).
[8] P. Burzynski *et al.*, Phys. Rev. A **90**, 022515 (2014).
[9] A. Lindblad, R. F. Fink, H. Bergersen, M. Lundwall, T. Rander, R. Feifel, G. Öhrwall, M. Tchaplyguinec, U. Hergenhahn, S. Svensson, and O. Björneholm, J. Chem. Phys. **123**, 211101 (2005).
[10] P. Lablanquie, S. Sheinerman, F. Penent, R. I. Hall, M. Ahmad, Y. Hikosaka, and K. Ito, Phys. Rev. Lett. **87**, 053001 (2001).
[11] B. Schütte, S. Bauch, U. Frühling, M. Wieland, M. Gensch, E. Plönjes, T. Gaumnitz, A. Azima, M. Bonitz, and M. Drescher, Phys. Rev. Lett. **108**, 253003 (2012).
[12] S. Bauch and M. Bonitz, Phys. Rev. A **85**, 053416 (2012).
[13] A. Niehaus, J. Phys. B **10**, 1845 (1977).
[14] A. Niehaus and C. J. Zwakhals, J. Phys. B **16**, L135 (1983).
[15] K. Helenelund, S. Hedman, L. Asplund, U. Gelius, and K. Siegbahn, Phys. Scr. **27**, 245 (1983).
[16] S. A. Sheinerman, J. Phys. B **27**, L571 (1994).
[17] G. B. Armen, J. Tulkki, T. Åberg, and B. Crasemann, Phys. Rev. A **36**, 5606 (1987).
[18] A. Russek and W. Mehlhorn, J. Phys. B **19**, 911 (1986).
[19] F. Robicheaux *et al.*, J. Phys. B **45**, 175001 (2012).
[20] Q. Wang, S. Sheinerman, and F. Robicheaux, J. Phys. B **47**, 215003 (2014).
[21] G. Sansone *et al.*, Science **314**, 443 (2006).
[22] E. Goulielmakis *et al.*, Science **320**, 1614 (2008).
[23] A. N. Artemyev, A. D. Müller, D. Hochstuhl, and Ph. V. Demekhin, J. Chem. Phys. **142**, 244105 (2015).
[24] A. N. Artemyev, A. D. Müller, D. Hochstuhl, L. S. Cederbaum, and Ph. V. Demekhin, Phys. Rev. A **93**, 043418 (2016).
[25] A. N. Artemyev, L. S. Cederbaum, and P. V. Demekhin, Phys. Rev. A **95**, 033402 (2017).
[26] A. N. Artemyev, L. S. Cederbaum, and P. V. Demekhin, Phys. Rev. A **96**, 033410 (2017).
[27] D. E. Manolopoulos and R. E. Wyatt, Chem. Phys. Lett. **152**, 23 (1988).
[28] T. N. Rescigno and C. W. McCurdy, Phys. Rev. A **62**, 032706 (2000).
[29] C. W. McCurdy, M. Baertschy, and T. N. Rescigno, J. Phys. B **37**, R137 (2004).
[30] E. Polizzi, Phys. Rev. B **79**, 115112 (2009).
[31] E. Polizzi and J. Kestyn, arXiv:1203.4031v3.
[32] A. Kramida, Y. Ralchenko, and J. Reader, *NIST Atomic Spectra Database* (National Institute of Standards and Technology, Gaithersburg, MD, 2012).
[33] The used carrier frequencies are slightly different from those expected from the presently computed IP and DIP of helium (i.e., $\omega_1 = \mathrm{IP} + \varepsilon_1 = 26.08\,\mathrm{eV}$ and $\omega_2 = \mathrm{DIP} + \varepsilon_2 = 64.42\,\mathrm{eV}$), which is due to short pulse durations and substantial energy dependencies of the respective photoionization transition amplitudes.
[34] See Supplemental Material at http://link.aps.org/supplemental/10.1103/PhysRevLett.122.183201, which contains animations of the one- and two-dimensional radial densities for the cases depicted in Fig. 2. Note that both pulses are polarized along the $z$ axis [see Eq. (1)]. In addition, Supplemental Materials contain animations of the photoelectron energy spectra depicted in Fig. 3.
[35] A. F. Starace, *Theory of Atomic Photoionization*, Handbuch der Physik (Springer, Berlin, 1982), Vol. 31.
[36] X. Wang and F. Robicheaux, Phys. Rev. A **98**, 053407 (2018).